ORIGINAL PAPER

Preparation of Porous Hollow SiO$_2$ Spheres by a Modified Stöber Process Using MF Microspheres as Templates

**Hui Liu · Hongliang Li · Zhaolong Ding · Aiping Fu ·
Hongyan wang · Peizhi Guo · Jianqiang Yu ·
Cunguo Wang · Xiu Song Zhao**

Abstract Using the surface charged and acid dissolvable melamine formaldehyde (MF) microspheres as sacrificial hard templates, silica coated MF core–shell composite microspheres, denoted as MF@SiO$_2$, were synthesized via a surfactant-assisted sol–gel process by using tetraethyl orthosilicate (TEOS) as silica source. Hollow SiO$_2$ spheres with mesoporous shells were then obtained after selective removal of the MF cores and the pore directing surfactant by hydrochloric acid etching or calcinations in air. Interesting shrinkage phenomena were observed in both the hollow products derived from hydrochloric acid etching and calcinations. The influence of the ratio of MF sphere to TEOS and the removal method of the MF core on the size of the hollow spheres, the shell thickness and the shell surface roughness have been studied. The composition, the thermal stability, the morphology, the surface area and pore size distribution, the wall thickness and adsorption properties of the hollow spheres derived from hydrochloric acid etching and calcinations were also investigated and compared based on the FTIR, SEM, TEM, TGA, Nitrogen adsorption–desorption and spectrophotometer techniques or measurements.

Keywords Hollow spheres · MF microspheres · Electrostatic assembly · Mesoporous materials

H. Liu · H. Li (✉) · A. Fu · H. wang · P. Guo · J. Yu · X. S. Zhao
Institute of Multifunctional Materials, Laboratory of New Fiber Materials and Modern Textile, Growing Basis for State Key Laboratory, College of Chemistry, Chemical Engineering and Environment, Qingdao University, Qingdao 266071, China
e-mail: lhl@qdu.edu.cn

Z. Ding · C. Wang
Key Lab of Rubber-plastics, Ministry of Education and Key Lab of Rubber-plastics of Shandong Province, Qingdao University of Science and Technology, Qingdao 266042, China

Introduction

Recently, the synthesis and preparation of hollow spherical materials has attracted more and more attention, not only for such materials compared with other materials, with a low density, large surface area, but also for a big hollow structure can accommodate a large number of guest molecules or large-size objects [1], therefore, the hollow microspheres have a number of potential applications in various fields such as photonics, catalysis, biotechnology, chromatography, the protection of biologically active agents, the controlled and timed drug delivery system, lightweight filter materials, chemical reactors and electrochemical cells etc. [2–7]. Numerous of chemical and physicochemical methods, such as heterophase polymerization combined with the sol–gel process, self-assembly techniques, template-sacrificial techniques, and chemically induced self-transformation, gas bubble assisted approach, spray-drying method, and layer-by-layer method have been developed to fabricate various hollow spheres [8–15]. Among them, template-sacrificial techniques, which can control the cavity size of hollow microspheres by selecting the size of templates are the most widely used and most effective method to the fabrication of hollow structures [16, 17]. Even though, this method still requires appropriate core templates and suitable coating process to fulfill the goals. Inorganic hollow spheres can be synthesized by which nanosized particles are coated on the surfaces of a template with certain charge and special functional groups by controlled precipitation of the inorganic precursor molecules, and then remove these templates through selective solvent etching or calcinations at high temperatures in air [18, 19]. The sacrificial template cores including hard templates (e.g., polymer latex, resin sphere, carbon) and soft templates (e.g., vesicles, ionic liquids, gas bubbles, and organogel), have been extensively employed [20–22].

During the last a few years, the weakly cross-linked melamine formaldehyde (MF) microspheres have been steadily exploited to the fabrication of functionalized polyelectrolyte multilayer-coated particles, hollow capsules and mesoporous carbon spheres, because of their monodisperse size, stable surface charge distribution, solubility in appropriate solvent and the volatile of calcined products [23–27], nevertheless little attention has been paid to the preparation of hollow spherical inorganic compounds by using MF spheres as templates [28]. Normally, hollow silica spheres with a mesoporous MCM-41 structure can be synthesized by using the layer-by-layer method [29], however, the synthesis procedure was relatively complicated and the obtained hollow spheres were not uniform in particle size. Moreover, the shell thickness of the hollow spheres is difficult to adjust [30]. In this article, we described a simple method to the fabrication of hollow silica spheres with porous wall based on the electrostatic assembly skill by using the hydrolyzation and condensation of TEOS occurring and then an in situ deposition process onto the surfaces of charged MF microspheres via a sol–gel process, respectively, obtaining firstly a silica-coated MF core–shell composites (denoted as MF@SiO$_2$), subsequently the hollow SiO$_2$ spheres after the selective removal of the organic MF core templates and the pore directing agent of CTAB from the MF@SiO$_2$ core–shell composite microspheres by HCl aqueous solution etching or high temperature calcinations in air. The composition, the morphology, the surface

area and pore size distribution, the wall thickness and the adsorption properties of the hollow spheres were also investigated.

Experimental Section

Materials

Formaldehyde (37%), melamine, polyvinyl alcohol (PVA), acetic acid, ammonia (28%), tetraethyl orthosilicate (TEOS, purity 99.8%), hydrochloric acid (HCl, 37%), absolute ethanol, Cetyltrimethyammonium bromide (CTAB). All the chemicals were of AR grade and used without further purification. Distilled water was used in all the experiments.

Synthesis of Monodisperse MF Microspheres

Monodisperse MF colloidal microspheres were prepared according to the literature with a modification [31]. Firstly, a solution of formaldehyde (5.3 mL, 37%) was mixed with melamine (2.8 g) under stirring at 60 °C for 20 min to obtain a clear precursor solution. When the resulting precursor solution was cooled down to 35 °C, then poured it into 90 mL PVA solution (0.4 wt%), obtaining a mixture. Consequently, acetic acid was introduced into the mixture until the pH value was adjusted to 4.5 and the solution was then kept at a stirring condition at 65 °C for 30 min to obtain MF colloidal particles. White MF spheres were collected by centrifugation, washed three times with water and ethanol, and finally dried in air at 60 °C.

Coating MF Microspheres with Silica

The coating reaction was directly processed at room temperature by a modified Stöber procedure, a commonly used sol–gel method to get amorphous silica. TEOS was used as silica source and a mixture of alcohol with water was used as solvent for the hydrolyzation of TEOS and also for the subsequent coating of MF microspheres with SiO$_2$. Ammonia was used as a catalyst for the hydrolyzation and Cetyltrimethylammonium bromide (CTAB) was utilized as the directing agent for the creation of pores in the wall of the final hollow spheres.

In a typical preparation, as-prepared MF microsphere (0.2 g) was added and well dispersed into absolute alcohol (100 mL) with the assistance of ultrasound irradiation for 15 min. Then the MF alcohol suspension was transferred into a round-bottomed flask, a solution containing cetyltrimethyl ammonium bromide (0.05 g), aqueous NH$_4$OH (1 mL) and water (1 mL) was added into the above suspension at room temperature within 20 min under magnetic stirring. Subsequently, A TEOS alcohol solution (15 mL, 1 vol%) was added into the above mixture with a constant flow pump, after that the reaction process was allowed to sustain for 5 h at room temperature under continuous stirring. The core–shell composite spheres were separated from the suspension by centrifugation and

washed three times with distilled water and ethanol. The solid was dispersed into an appropriate volume of deionized water and cooled to freeze; white powder, denoted as MF@SiO$_2$, was then obtained after a 24 h freeze-drying process on a FD-1A-50 freeze-dryer and was preserved for subsequent experiments.

Preparation of Hollow SiO$_2$ Spheres

Silica hollow microspheres with a porous wall were obtained after a heat-treatment of the MF@SiO$_2$ composites in a programmed muffle furnace at 550 °C for 3 h in air with a heating rate of 1 °C/min or by HCl aqueous solution (pH 1) etching at room temperature to remove the MF cores and the CTAB pore directing agents.

Adsorption Tests

To determine the adsorption properties of the hollow spheres, a 10.7 mg methylene blue, which was used as a model adsorbate sample, was dissolved in 250 mL distilled water. After the methylene blue dissolved completely, 0.1 g hollow spheres were added into the solution and stirred for several minutes, the suspension was then left to stand. At time intervals, 3.0 mL of the upper solution was withdrawn and immediately replaced with an equal volume of fresh H$_2$O to keep the volume constant. The withdrawn samples were properly diluted and analyzed by a UV–Vis spectrophotometer to determine the concentration of methylene blue in the solvent, then converted into the mass of methylene blue. Finally, the quantity of the absorbed methylene blue at a time was obtained by a computational formula:

$$M_B(mg/g) = (m_B - m)/m_o,$$

M_B is the quantity of adsorbed methylene blue (mg/g), m_B is the initial mass of methylene blue (mg), m is the residual mass of methylene blue in the solvent (mg), m_o is the mass of hollow spheres (g).

Characterization

The morphologies and the structures of the samples were examined by a JEOL JSM-6390LV scanning electron microscopy (SEM) and a JEM-2010F transmission electron microscopy (TEM). The thermal stability of the pristine MF sphere and the MF@SiO$_2$ composite were studied by thermogravimetric analysis (TGA-DSC, STA 449C). The specific surface areas were estimated using the Brunauer–Emmett–Teller (BET) method with a TriStar 3000 Surface Area and Pore Analyzer (Micromeritics). Fourier transformation infrared (FTIR) spectra were recorded with a Nicolet 5700 FTIR spectrometer on KBr pellets. Powder X-ray diffraction (XRD) patterns were collected using a Bruker D8 advance X-ray diffractometer equipped with graphite monochromatized Cu Kα radiation ($\lambda = 0.15418$ nm). UV–Vis spectra were measured through a TU-1901 UV–Visible spectrophotometer.

Results and Discussion

FT-IR Spectra

Two different processes were applied to remove the MF cores to get the hollow SiO$_2$ spheres (see "Experimental Section"). The FTIR spectra of the pristine MF spheres, MF@SiO$_2$ core–shell composites and the corresponding hollow SiO$_2$ spheres were measured and compared in order to confirm the formation of the MF@SiO$_2$ composites and the complete removal of the MF cores after the calcination or etching.

Curves A and B in Fig. 1 show the characteristic absorption bands of MF at about 3377, 1557 (1492, 1352), 1166, 1006 and 813 cm^{-1} originating from the vibrations of hydroxyl/amino (–OH/–NH$_2$), amino (–NH$_2$), amine (C–N), ether (C–O–C), and C–N–C groups, respectively [32]. The broad peak at around 1100 cm^{-1} in curves B, C and D can be attributed to the Si–O–Si asymmetric bond stretching vibration, and the bands at 953 cm^{-1} can be assigned to the Si–OH stretching vibration. The peaks around 3450 and 1630 cm^{-1} are attributed to the O–H stretching vibration and the bending vibration of the –OH group of the silanols moieties and the adsorbed water molecules. However, after HCl etching (curve C) and calcinations (curve D), the absorbance peaks of MF disappeared, indicating that on the one hand the MF cores have been removed after the process of HCl aqueous solution etching or calcinations, furthermore, which provides evidence on the other hand to the formation of the MF@SiO$_2$ composite and pure silica. Moreover, the Si–O–Si asymmetric bond stretching vibration band at about 1077 cm^{-1} decreases in intensity (compare curve D with curve C) due to a more open SiO$_2$ network structure with lower internal stress formed in the calcination process.
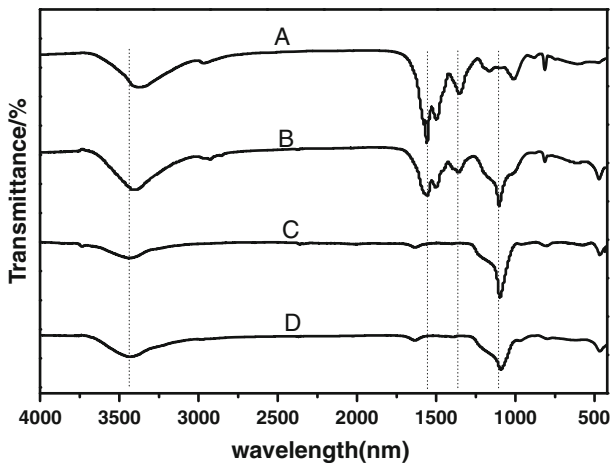

Fig. 1 FTIR spectra of pure MF microspheres (*a*), the core–shell-structured composite (*b*), and SiO$_2$ hollow spheres derived by HCl aqueous solution etching (*c*) and high temperature calcinations (*d*), respectively

Thermogravimetric Analysis

The thermogravimetric analysis (TGA) results of the pure MF sphere template and the core–shell structured composite are illustrated in Fig. 2 as curve A and curve B, respectively. From the curves we can see that the pure MF spheres and the MF@SiO$_2$ composites show quite similar weight loss behavior. There are three main stages of weight loss in both the curves: the first weight loss can be observed from the curves in the range of 50 and 100 °C, which may be caused by the desorption of the absorbed water on the surfaces of the samples, whereas the second weight loss between 100 and 250 °C can be attributed to the dehydration and densification of the MF templates and the amorphous silica. The ultimately rapid weight losses from about 350 °C can be assigned in curve A to the burning of the MF spheres and that in curve B to the combination of the burning of MF templates and the condensation of the amorphous silica for the MF@SiO$_2$ composite spheres. From curve A, one can see that the weight loss of the pure MF template is nearly 100%, indicating that the MF template can be removed completely after calcinations. In comparison of curve A with curve B, it can also be derived that the weight percentage of silica composite in the MF@SiO$_2$ composite is about 12.8%. The TGA results provide us also information for selecting calcinations temperature to remove the MF core from the core–shell composites and temperature increase rate to avoid the broken of the hollow products. The ruptured hollow sphere (see inset in picture B of Fig. 4) indicates that one must control the calcinations temperature and heating rate during the calcination process to avoid the releasing of gaseous carbon/nitrogen oxides to break through the shells.

SEM Measurements

SEM measurements have been carried out to investigate the morphologies of the samples. Picture A in Fig. 3 shows the SEM image of the pure MF microspheres,
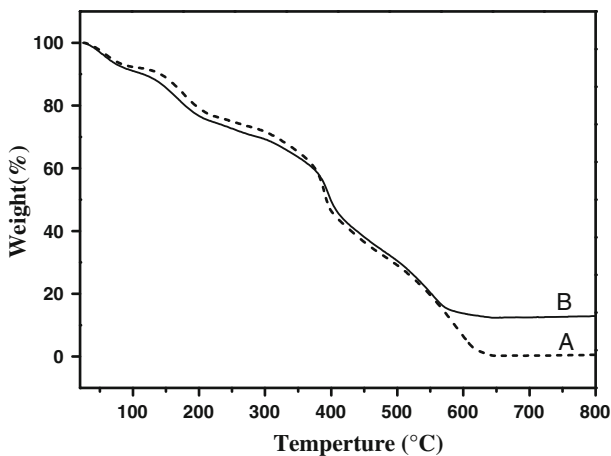

Fig. 2 TGA curves of the pure MF spheres (*dashed line, a*) and that of the as-dried MF@SiO$_2$ core–shell particles (*solid line, b*)

which was used as template cores in the preparation of the core–shell composites and the corresponding hollow spheres. It can be seen that the MF templates with a smooth surface texture consist of highly uniform and well-dispersed microspheres with mean diameter of about 1.2 μm. Pictures B–E in Fig. 3 show the SEM images of the MF@SiO₂ composite microspheres fabricated with different ratio of TEOS precursors. From the pictures one can clearly see that the mean diameter of the core–shell composite increases obviously with the addition ratio of TEOS precursor increased from 1–6 vol%, meanwhile, the surfaces of the composite microspheres become rough. It can also be seen that separated silica particles arched on the surface of the composites spheres (see pictures D and E) and even isolated agglomerates of silica spheres (see picture E) have been formed with the increasing of the TEOS concentration. The increase of the average diameter and the surface roughness of the composite microspheres with the increasing of the TEOS quantity disclosed that a silica shell has been coated onto the core of MF microspheres during the in situ hydrolysis, condensation and coating process. That means also the thickness of silica coating layer can be tuned conveniently by varying the quantity of the TEOS precursors, and on the other hand that the ratio of MF core to TEOS precursor should be controlled below a value in order to obtain a uniform silica shell. The size and the morphology of the hollow spheres derived from the corresponding MF@SiO₂ composites mentioned above after calcinations are studied with SEM and been showed and compared in Fig. 4. It is very interesting that spheres with mean diameters of about 200, 400 and 700 nm were obtained when 1–3 vol% of TEOS were utilized, respectively, even with the same sized MF core templates (see Pictures A–C). Obviously, a shrinkage of the silica coating layer and the MF core was took place during the calcinations treatments, which can be explained as due to the dehydration of the MF templates and the densification of the loose outer coating shell which caused the formation of a compact silica wall finally. The inset in picture B shows a broken sphere after the calcinations treatment, revealing the hollow properties of the spheres.

TEM Studies

The morphologies, the hollow properties and the thickness of the silica wall were characterized further by transmission electron microscopy (TEM). The images as showed in Fig. 5 are the hollow spheres obtained by calcinations (A, C) and hydrochloric acid solution etching (B, D) and were derived from MF@SiO₂ composites made of 1 vol % (A, B) and 3 vol % (C, D) of TEOS precursors, respectively. From pictures A and B one can see that the spheres with sizes of about 200–300 nm were obtained after the removal of the MF cores. With the increasing of TEOS precursors, both the size and the wall thickness of the hollow spheres increase and hollow spheres with size of about 500–700 nm were obtained when 3 vol% TEOS precursor was used (see pictures C and D in Fig. 5). All of the hollow spheres derived from different amount of TEOS and different MF core removal method are much smaller than that of the MF@SiO₂ composites and even the MF cores themselves. One can also find that the thickness of the shells derived from calcinations is more thick and much condensed than that derived from the HCl solution etching, however, a shrinkage of the shell took place for both the
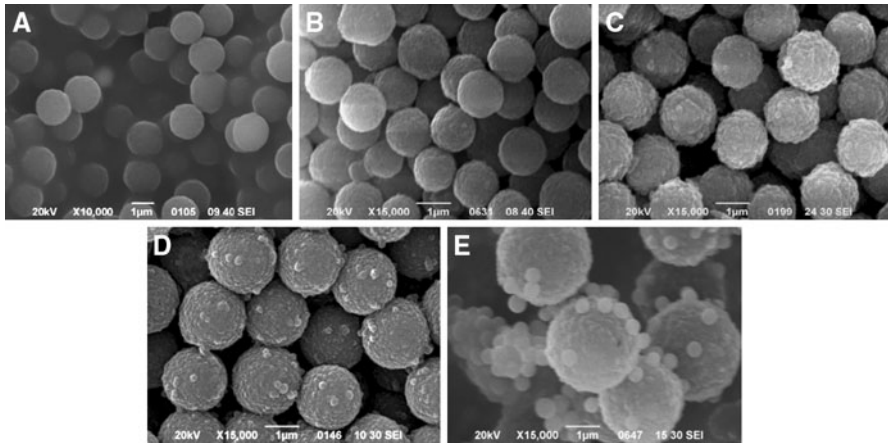
Fig. 3 SEM images of pure MF microspheres (**a**), and MF@SiO$_2$ composite microspheres derived from various of TEOS ratio, **b** 1 vol%, **c** 2 vol%, **d** 3 vol%, **e** 6 vol%
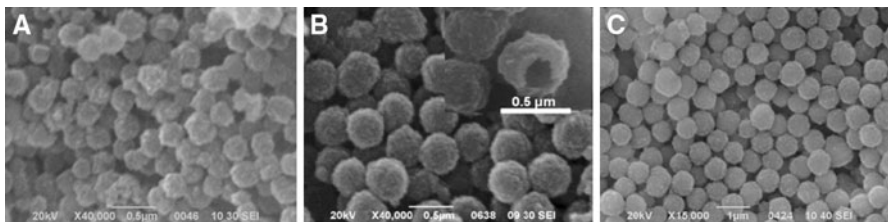

Fig. 4 SEM images of the Hollow SiO$_2$ microspheres derived from the MF@SiO$_2$ composites (**a** 1 vol%, **b** 2 vol% and **c** 3 vol% TEOS ratio, respectively) by calcinations

calcinations and the acid solution etching processes. The shrinkage of the silica coating layer and the MF core during the former process can be attribute to the dehydration of the MF templates and the densification of the loose outer coating shell, which caused the formation of a compact silica wall finally, however, the shrinkage in the latter treatment is a little bit difficult to be understood, and the shrinkage might took place during the dry process after the etching. More detailed study on the shrinkage mechanism is still underway. The shrinkage phenomena occurred during the template removal process and the shrinkage percentage of the hollow sphere in comparison with the MF@SiO$_2$ core–shell sphere, which were related to the amount of the added TEOS, provide another possibility to control the size of the final products, especially for the preparation of small sized hollow spheres, which is required, for example, for drug delivery applications.

Nitrogen Adsorption–Desorption Measurements

The N$_2$ adsorption–desorption measurements were carried out to determine the specific surface area and pore size distributions of the porous hollow SiO$_2$ spheres.
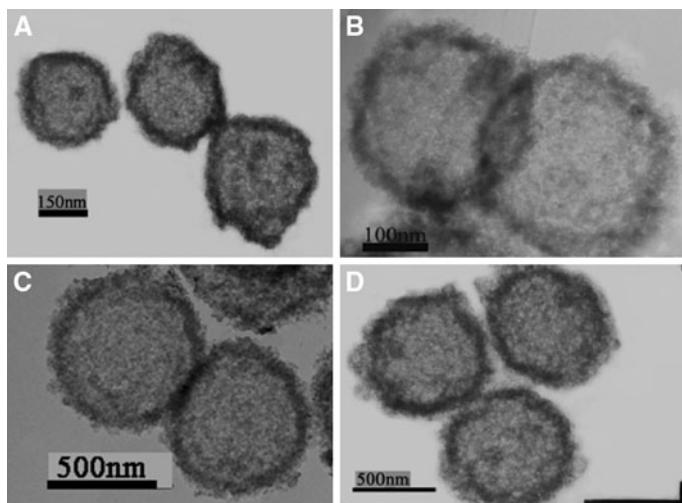
Fig. 5 TEM images of hollow SiO₂ spheres made of (**a**, **b**) 1 vol% and (**c**, **d**) 3 vol% TEOS precursors after the removal of the MF cores by calcinations (**a**, **c**) and HCl aqueous solution etching (**b**, **d**), respectively

The isotherms and corresponding pore size distributions were shown in Fig. 6. Both the samples obtained by calcinations and acid etching methods contain hysteresis loops that can be classified as type IV isotherms characteristic of porous structures. The isotherms of the samples obtained by HCl etching (panel (a) of Fig. 6) and calcinations (panel (b) of Fig. 6), respectively, were calculated via the Barret-Joyner-Halenda (BJH) method, which present BET surface area of $882 \text{ m}^2\text{g}^{-1}$ and pore size distribution centered at about 2.2 nm for the former, and specific surface area of $471 \text{ m}^2\text{g}^{-1}$ and pore size distribution of about 10.5 nm for the latter. Such a large specific surface area is mainly arisen from their pores in the wall and also possibly resulted partially from its rough nanostructures of the external surfaces. The shapes of the hysteresis loops for the samples derived from the acid etching and the calcinations are different, which could be involved with the texture differences of the mesoporous silica wall. In panel (a) of Fig. 6, this type of hysteresis loop is extraordinarily narrow and steep at p/p_0 0.1–0.3, which shows obviously capillary condensing phenomenon, but a wide hysteresis loop at p/p_0 0.3–1 indicating a typical hollow sphere with mesopores. In panel (b) of Fig. 6, the hysteresis loop displays the isotherms characteristic of mesoporous materials in the relative high pressure range of 0.7–1 p/p_0. The hysteresis loop in isotherm of Fig. 6a is mainly attributed to the interparticle spacing between the silica particles. During a process of HCl etching, the MF cores were dissolved by the HCl aqueous solution, meanwhile, the CTAB surfactant inside the silica shell can also be dissolved and be rinsed out, forming the internal hole and the pores in the silica shell. Furthermore, the reaction between hydrochloric acid and unhydrolytic Si–OH groups, which will deplete part of the Si–OH groups, and the consequent low temperature dry process, which

can give rise to partial condensation reaction of the Si–OH group, can introduce also small sized mesopores in the silica wall. The factors account for isotherm of Fig. 6b as following, first, with the surfactants CTAB removing by calcinations at high temperatures in air, the large mesopores in the wall can then be constructed, however, calcinations prompted also the more dense shell and made the mesopores that caused by interparticle spacing reduced, therefore, hollow spheres with large pore but less specific surface area were deduced.
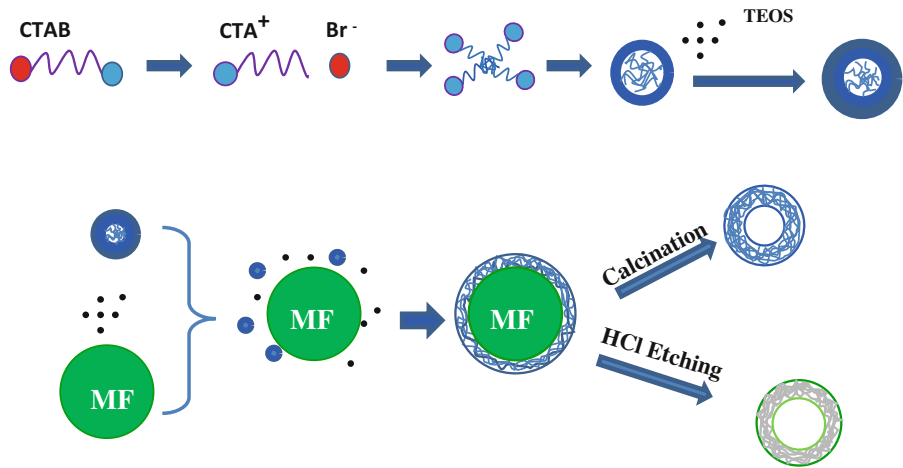
Formation Mechanism

A proposed formation mechanism of the hollow structures was schemed in Fig. 7. Firstly, the surfactant CTAB in the water–ethanol–ammonia mixture hydrolyzed and produced cationic CTA^+, and then the cationic CTA^+ self-assembly, forming micelles. Afterwards, the hydrolysis and condensation reactions of the TEOS produced soluble SiO_2 nucleus in an alkali condition, and they occurred adsorption with cationic CTA^+ micelles based on the electrostatic induced assembly, forming $CTAB/SiO_2$ grains with negative charged surface and then the grains self-assemble again onto the surface of the positively charged MF spheres, forming SiO_2 packed MF core–shell composite spheres (MF@SiO_2) via an electrostatic adsorption. Finally, Hollow SiO_2 spheres were obtained after selective removal of the organic MF core by HCl solution etching or calcinations in air. During the calcinations or the acid etching process, shrinkage of the silica shell took place in order to form a complete and condense shell structure, resulting in hollow spheres with size less than that of the MF core template.

Adsorption Property

Two main issues need to be addressed concerning the possible application of the porous hollow silica spheres fabricated in this article as absorber or guest vectors.
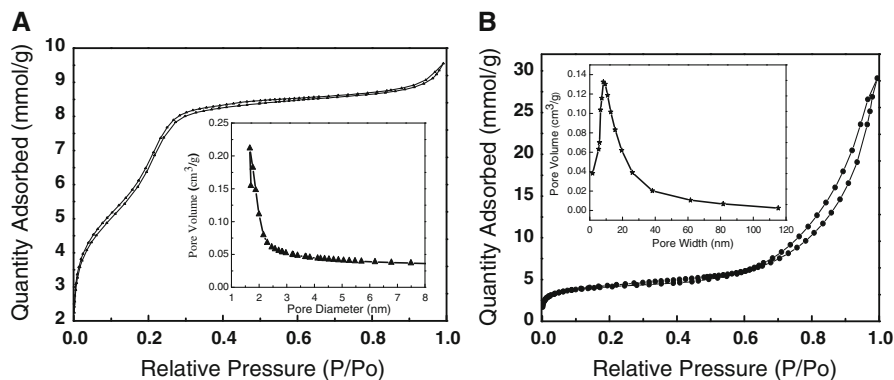

Fig. 6 Nitrogen adsorption–desorption isotherms and the corresponding pore-size distributions (the *inset*) of the hollow SiO_2 spheres with equivalent amount of TEOS (3 vol%) but different core removal methods, **a** HCl etching; **b** calcinations

Fig. 7 Schematic diagram of formation mechanism of the hollow spheres

First, sphere size is important because the ability of the spheres to reach a given location for example in the body as drug carriers is limited by the size of the vessels of the human circulatory system. Secondly, the surface area and the pore size distribution play also crucial role to its practical application. The above results and discussion demonstrated that the hollow-structured mesoporous silica spheres have a relative large specific surface area and with plentiful mesosized pores. In our cases, the size of the hollow spheres can be tuned by adjusting the addition amount of the TEOS precursors, while the specific surface area and the pore size distributions can be modified by using different MF core removal method. The adsorption ability of the porous hollow spheres derived from acid etching and calcinations, respectively, were investigated and compared using methylene blue as a model adsorbate. Figure 8 shows the adsorption behaviors of the two types of hollow porous silica spheres with different specific surface area and pore size distributions, in which the concentration of the model adsorbate was monitored by a UV–Visible spectrophotometer. From the curves one can find that the sample (curve A) derived from acid etching with a specific surface area of about 882 m²/g and pore size distribution of about 2.2 nm, achieved the adsorption balance in about 45 min and showed a maximum adsorption amount of about 79 mg/g, while, sample (curve B) made by the calcinations reached the equilibrium state in about 30 min with the ceiling amount of adsorption capacity at about 70 mg/g, which showed shorter adsorption equilibrium time but a smaller adsorption capacity than the former sample. The difference between these two types of samples can be explained as due to the larger specific surface area for the former, which is involved to the adsorption capacity, and the larger pore size for the latter, which made an adsorption equilibrium state much easier than the former. Hence, we concluded that for some applications, the specific surface area and the pore size distributions should have an optimized value range.
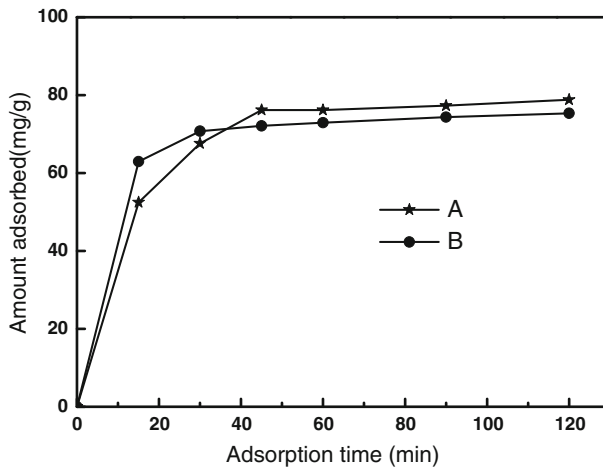
Fig. 8 Adsorption kinetics of methylene blue on the hollow-structured mesoporous spheres derived from HCl etching (*a*) and calcinations (*b*), respectively

Conclusions

Hollow silica spheres with a mesoporous wall have been successfully fabricated after the removal of the MF templates and the CTAB additives in the $MF@SiO_2$ core–shell composite, which were prepared firstly by using MF as sacrificial core and combining a surfactant-assisted sol–gel process, by HCl etching and high temperature calcinations. The size of the hollow spheres, the specific surface area, pore size distribution in the wall and the shell thickness of the hollow spheres can be manipulated by tuning the concentration of the TEOS solution and by selecting the MF template removal method. Interesting shrinkage phenomena occurred during the template removal processes, and the shrinkage percentage of the hollow sphere in comparison with the $MF@SiO_2$ core–shell sphere was related to the amount of the added TEOS, which provides another possibility to control the size of the final products, especially for the preparation of small sized hollow spheres. Hollow mesoporous silica spheres derived from HCl etching and high temperature calcinations of the $MF@SiO_2$ core–shell composite show different specific surface area valves and different pore size distributions. The specific surface area and pore size distribution can influence obviously on the adsorption capacity and adsorption equilibrium time. Further development of the hollow spheres, for example, endowing the porous hollow spheres with magnetic properties will extend the application of this novel structure.

References

1. H. S. Im, U. Jeong, and Y. Xia (2005). *Nat. Mater.* **4**, 671.
2. P. Yang, S. Gai, Y. Liu, W. Wang, C. Li, and J. Lin (2011). *Inorg. Chem.* **50**, 2182.
3. X. Wang, P. Gao, and J. Li (2002). *Adv. Mater.* **14**, 1732.
4. J. X. Xu, G. J. Chen, R. Yan, D. Wang, and P. C. Sun (2011). *Macromolecules* **44**, (10), 3730.
5. Y. Yamada, T. Nakamura, M. Ishi, and K. Yano (2006). *Langmuir* **22**, 2444.
6. B. J. Melde, B. J. Johnson, and P. T. Charles (2008). *Sensors* **8**, 5202.
7. Q. Zhang, T. Zhang, J. Ge, and Y. Yin (2008). *Nano Lett.* **8**, 2867.
8. J. Yu, X. Yu, B. Huang, and X. Zhang (2009). *Cryst. Growth Des.* **9**, 1474.
9. J. Yang, J. U. Lind, and W. C. Trogler (2008). *Chem. Mater.* **20**, 2875.
10. H. C. Zeng (2006). *J. Mater. Chem.* **16**, 649.
11. H. G. Yu, J. G. Yu, S. W. Liu, and S. Mann (2007). *Chem. Mater.* **19**, 4327.
12. X. Sun, J. Liu, and Y. Li (2006). *Chem. Eur. J.* **12**, 2039.
13. K. Akamatsu, W. Chen, Y. Suzuki, and T. Ito (2010). *Langmuir* **26**, (18), 14854.
14. X. F. Qu, Q. Z. Yao, G. T. Zhou, and S. Q. Fu (2010). *J. Phys. Chem. C* **114**, 8734.
15. W. Leng, M. Chen, S. Zhou, and L. Wu (2010). *Langmuir* **26**, (17), 14271.
16. T. Zhang, Q. Zhang, J. Ge, and J. Goebl (2009). *J. Phys. Chem. C* **113**, 3168.
17. H. Hu, H. Zhou, J. Liang, An. Lu, and H. X. Wu (2011). *J. Colloid Interface Sci.* **358**, 392.
18. Z. Deng, M. Chen, S. Zhou, and B. You (2006). *Langmuir* **22**, 6403.
19. A. Schmid, S. Fujii, and S. P. Armes (2006). *Langmuir* **22**, 4923.
20. P. Hu, L. Yu, A. Zuo, C. Guo, and F. Yuan (2009). *J. Phys. Chem. C* **113**, 900.
21. J. G. Yu, H. Guo, S. A. Davis, and S. Mann (2006). *Adv. Funct. Mater.* **15**, 2035.
22. Y. Q. Ye, B. C. Chen, H. P. Lin, and C. Y. Tang (2006). *Langmuir* **22**, 6.
23. K. Szczepanowicz, D. Dronka-Góra, G. Para, A. M. Bouzga, C. Simon, and Juan. Yang (2009). *Procedia Chem.* **1**, 1576.
24. X. Shi, A. L. Briseno, R. J. Sanedrin, and F. Zhou (2003). *Macromolecules* **36**, 4093.
25. W. Li, D. Chen, Z. Li, Y. Shi, and Y. Wan (2007). *Electrochem. Commun.* **9**, 569.
26. W. S. Choi, H. Y. Koo, and D. Y. Kim (2008). *Langmuir* **24**, 4633.
27. G. Jia, H. You, Y. Song, Y. Huang, M. Yang, and H. Zhang (2010). *Inorg. Chem.* **49**, 7721.
28. G. Jia, H. P. You, K. Liu, Y. H. Zheng, N. Guo, and H. J. Zhang (2010). *Langmuir* **7**, 5122.
29. S. Sadasivan and G. B. Sukhorukov (2006). *J. Colloid Interface Sci.* **304**, 437.
30. Y. S. Zhao, H. Wang, Y. M. Liu, J. L. Ye, and S. G. Shen (2008). *Mater. Lett.* **62**, 4254.
31. Z. L. Ding, H. L. Li, and C. G. Wang (2011). *J. Funct. Mater.* **42**, (Suppl III), 492.
32. B. Friedel and S. Greulich-Weber (2006). *Small* **2**, 859.